

Research paper

Ultrathin MoS₂ layers anchored exfoliated reduced graphene oxide nanosheet hybrid as a highly efficient cocatalyst for CdS nanorods towards enhanced photocatalytic hydrogen production



D. Praveen Kumar, Sangyeob Hong, D. Amaranatha Reddy, Tae Kyu Kim*

Department of Chemistry and Chemical Institute for Functional Materials, Pusan National University, Busan 46241, Republic of Korea

ARTICLE INFO

Article history:

Received 26 December 2016

Received in revised form 18 April 2017

Accepted 24 April 2017

Available online 25 April 2017

Keywords:

Photocatalysis

Hydrogen

Exfoliation

MoS₂

CdS

Reduced graphene oxide

ABSTRACT

The development of novel highly efficient noble metal-free co-catalysts for enhanced photocatalytic hydrogen production is of great importance. Herein, we report the synthesis of novel and highly efficient noble metal-free ultra-thin MoS₂ (UM) layers on exfoliated reduced graphene oxide (ERGO) nanosheets as a cocatalyst for CdS nanorods (ERGO/UM/CdS). A simple method different from the usual preparation techniques is used to convert MoS₂ to UM layers, graphene oxide (GO) to ERGO nanosheets, based on ultrasonication in the absence of any external reducing agents. The structure, optical properties, chemical states, and dispersion of MoS₂ and CdS on ERGO are determined using diverse analytical techniques. The photocatalytic activity of as-synthesized ERGO/UM/CdS composites is assessed by the splitting of water to generate H₂ under simulated solar light irradiation in the presence of lactic acid as a hole (h⁺) scavenger. The observed extraordinary hydrogen production rate of ~234 mmol h⁻¹ g⁻¹ is due to the synergistic effect of the ultrathin MoS₂ layers and ERGO, which leads to the effective separation of photogenerated charge carriers and improves the surface shuttling properties for efficient H₂ production. Furthermore, the observed H₂ evolution rate is much higher than that for individual noble metal (Pt), ERGO and MoS₂-assisted CdS photocatalysts. Moreover, to the best of our knowledge, this is the highest H₂ production rate achieved by a RGO and MoS₂ based CdS photocatalyst for water splitting under solar light irradiation. Considering its low cost and high efficiency, this system has great potential for the development of highly efficient photocatalysts used in various fields

© 2017 Elsevier B.V. All rights reserved.

1. Introduction

Solar-light Conversion of solar energy into alternative sustainable chemical fuels is considered one of the major strategies to address the energy crisis and tackle environmental problems [1,2]. Ever since Fujishima and Honda reported hydrogen production by photoelectrocatalytic water splitting using a TiO₂ electrode [3], this process has attracted much attention as it is a promising approach for clean, low-cost, and environmentally friendly hydrogen production utilizing solar energy [4,5]. To date, several types of photocatalytic materials have been developed, such as mixed transition metal oxides, titanate, niobate, and tantalate; however, these bare materials exhibit limited utilization of visible light radiation. However, visible light accounts for the major part of the

incoming solar energy [6–10], necessitating the exploration of visible light-driven photocatalysts.

Among the various visible light-active semiconductor photocatalysts, CdS has proven to be a suitable candidate for photocatalytic water splitting due to its well-suited band gap of ca. 2.4 eV that accounts for the excellent excitation of charge carriers via effective sunlight absorption. The conduction band edge potential of CdS is more negative than the reduction potential of H₂O/H₂, favoring the reduction of protons (H⁺) to H₂ gas [11,12]. However, bare CdS exhibits a limited rate of H₂ production due to its fast charge carrier recombination and susceptibility to photocorrosion [13]. One-dimensional (1D) CdS nanostructures can be used to overcome these problems, exhibiting a unidirectional flow of photoexcited charge carriers and a relatively short surface transfer path [14], although their activity is still low. Integration of co-catalysts into 1D CdS semiconductor materials has proven to be an effective approach for enhancing photocatalytic H₂ generation. Generally, the hydrogen evolution activity can be efficiently enhanced by deposition of noble metals such as Pt, Pd, Au, and Rh, which

* Corresponding author.

E-mail address: tkkim@pusan.ac.kr (T.K. Kim).

have been extensively used as co-catalysts [15–18]. However, the use of noble metals in practical applications is largely restricted by their high cost and low abundance [19,20]. It is therefore highly desirable to replace noble metals with low-cost materials for the development of highly efficient photocatalysts. Recently, the use of two-dimensional (2D) layered materials in photocatalytic applications has gained popularity due to their extraordinary advantages, such as the large surface area and excellent catalyst support properties. Some typical 2D layered materials such as graphene, MoS₂, and g-C₃N₄ have been recognized as promising candidates for photocatalytic applications [21–24]. Moreover, semiconductor photocatalysts based on 2D layered materials with different compositions have been developed due to their advantageous properties. These composites represent a new kind of photocatalysts for redox reactions, showing improved performance and fast transfer/separation rates of the photogenerated electrons and holes with no recombination. In this regard, MoS₂ is the most attractive of the 2D layered materials due to its peculiar properties. In general, MoS₂ exhibits a sandwich structure featuring three stacked atomic layers (S–Mo–S) linked by van der Waals forces and has been frequently used in photocatalysis [25–27]. Moreover, the density functional theory calculation of free energies shows that the S atoms on the exposed edges of MoS₂ form strong bonds to H⁺ in solution that are easily reduced to H₂ by electrons. Theoretically, the cocatalytic activity of MoS₂ is caused only by the active S atoms on its exposed edges, with the majority of S atoms in the basal plane being inactive [26,28]. Therefore, conversion of MoS₂ nanosheets into ultrathin nanosheet layers with a large number of exposed active sites increases its activity [29,30]. A very recently, we reported ultrathin MoS₂ decorated CdS nanorods catalyst for photocatalytic hydrogen production [31]. In this report we found that, it is an important to both synthesize efficient materials and use them efficiently to obtain spectacular rate of H₂ production. Besides there is an open door to farther over again improve the photocatalytic activity of ultrathin MoS₂ based CdS composites, by improving electrical conductivity of ultrathin MoS₂ layers. For even the ultrathin MoS₂ layers feature a large number of exposed active sites, their co-catalytic activity is partially restricted due to the poor electrical conductivity and it is insufficient to effective charge carrier mobility.

Furthermore, the electrical conductivity and activity of MoS₂ can be improved by introduction of other conductive materials [32,33]. Graphene oxide (GO) has attracted much attention owing to unique features such as its large specific surface area (SSA), superior electron mobility, excellent electronic behavior, and high stability, being widely used as a photocatalyst and/or cocatalyst for H₂ production [34–36]. However, the produced GO sheets are prone to agglomeration or restacking because of the strong van der Waals interactions. These effects result in a low electrochemically active surface area, small interlayer spacing, and low electrical conductivity. Hence, the electrical conductivity of GO nanosheets is dramatically improved by exfoliation into separated layers simultaneous conversion of RGO [37–42]. There is diverse techniques [43] are existing to covert GO into RGO such as; reduction by reducing agent, photo reduction, solvothermal and ultrasonication methods [43,44]. In addition, Plenty of reports for conversion of GO to RGO is utilized hydrazine, but it is very toxic to humans and the environment, it is highly explosive and poisonous, when used in large quantities [45]. Among these techniques, ultrasonication process stands in top due to its simplicity, ecofriendly and simultaneous exfoliation of layers [44]. According to earlier reports [46], RGO/MoS₂ based composites exhibit higher co-catalytic activities on CdS than pure MoS₂ and RGO separately, implying that using MoS₂/RGO hybrid as co-catalyst can efficiently suppress charge carrier recombination, improve interfacial charge transfer, and enhance photocatalytic activity. Except simple RGO/MoS₂; ultra-

thin MoS₂/exfoliated RGO hybrid as highly efficient co-catalyst to improve the activity of CdS nanorods due to large number of exposed active sites as well as higher electrical conductivity. These double advanced benefits are offered to superior rate of H₂ production to CdS catalyst. Moreover this system is noble metal free and it can be utilize visible light, further improving the efficiency of solar energy conversion.

Herein, we report the facile synthesis of CdS nanorods decorated by ultra-thin MoS₂ layers on exfoliated reduced graphene oxide nanohybrid (ERGO/UM/CdS). The photocatalytic hydrogen evolution activities of the synthesized materials were tested under natural solar light irradiation at optimal conditions, with lactic acid as hole-scavenger. The optimized ERGO/UM/CdS exhibited a high H₂ production rate (234 mmol h⁻¹ g⁻¹). The ERGO/UM nanohybrid cocatalysts on the surface of CdS nanorods effectively separate the photogenerated charge carriers and improve the surface shuttling properties for efficient H₂ production due to their highly active edge sites with superior electrical conductivity. To the best of our knowledge, this material shows the best performance among all reported MoS₂, RGO, and MoS₂/RGO cocatalyzed CdS composites (Table S1 in Supporting Information (SI)).

2. Experimental and characterizations

2.1. Materials

Cadmium acetate dihydrate ($\text{Cd}(\text{CH}_3\text{COO})_2 \cdot 2\text{H}_2\text{O}$), sodium molybdate dihydrate ($\text{Na}_2\text{MoO}_4 \cdot 2\text{H}_2\text{O}$), and ethanol were purchased from Daejung Chemicals & Metals Co., Ltd., Korea. Thiourea (NH_2CSNH_2) and thioacetamide ($\text{C}_2\text{H}_5\text{NS}$) were obtained from Alfa Aesar. All chemicals were used without further purification.

2.1.1. Synthesis of ERGO/UM/CdS nanocomposites

1D CdS nanorods, GO and bulk MoS₂ nanosheets were synthesized separately using different methods. GO and MoS₂ nanosheets were converted into exfoliated RGO and ultrathin MoS₂ nanosheets respectively then intercalated onto CdS nanorods by ultrasonication followed by distillation. A schematic representation of the synthesis procedure is shown in **Scheme 1**, and details of the synthetic procedures are given in the experimental part of SI.

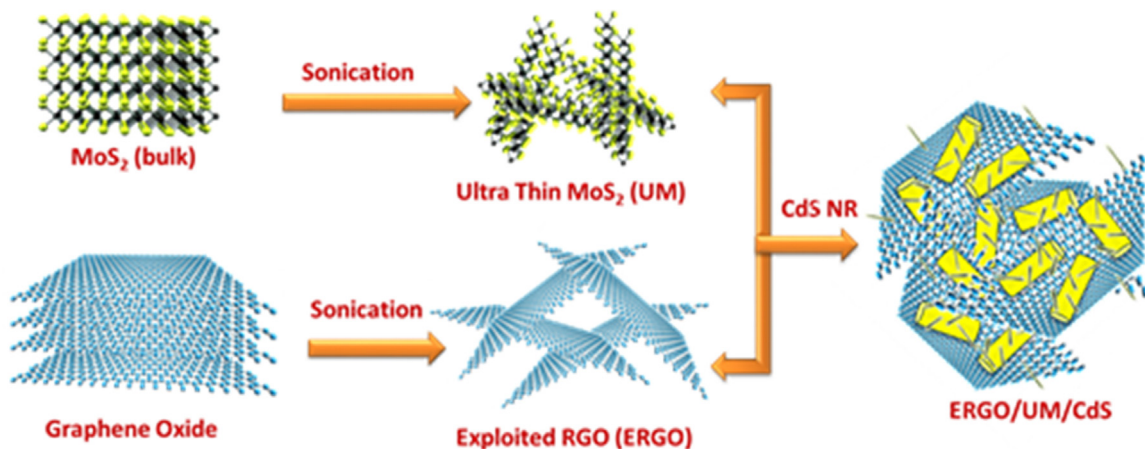
3. Results and discussion

3.1. Structural analyses

To The phases of the as-synthesized materials were investigated by X-ray diffraction (XRD). As shown in **Fig. 1(a)**, the diffraction patterns of pure CdS nanorods (CdS) and their composites correspond to a hexagonal structure (JCPDS card No. 89-2944), with no typical peaks of MoS₂ and exfoliated reduced graphene oxide (ERGO) detected, which is ascribed to the relatively low content and weak diffraction intensity of ERGO and MoS₂ [47]. Furthermore, the XRD patterns confirm the conversion of pristine graphite to graphene oxide (GO) and bulk MoS₂ to ultrathin MoS₂ (**Fig. S1** in SI), in agreement with previous reports [46].

3.2. Surface elemental analysis

The X-ray photoelectron spectroscopy (XPS) is a particularly useful tool for studying the surface composition and electronic structure of materials, providing information on the chemical environment of the elements in the synthesized composites. XPS analysis was performed to determine the chemical states of Cd, Mo, C, O, and S in the as-prepared ERGO/UM/CdS composite, with results displayed in **Fig. 1(b)–(f)**. XPS survey spectra reveal the pres-



Scheme 1. Schematic representation of materials preparation: ERGO/UM/CdS nanocomposites.

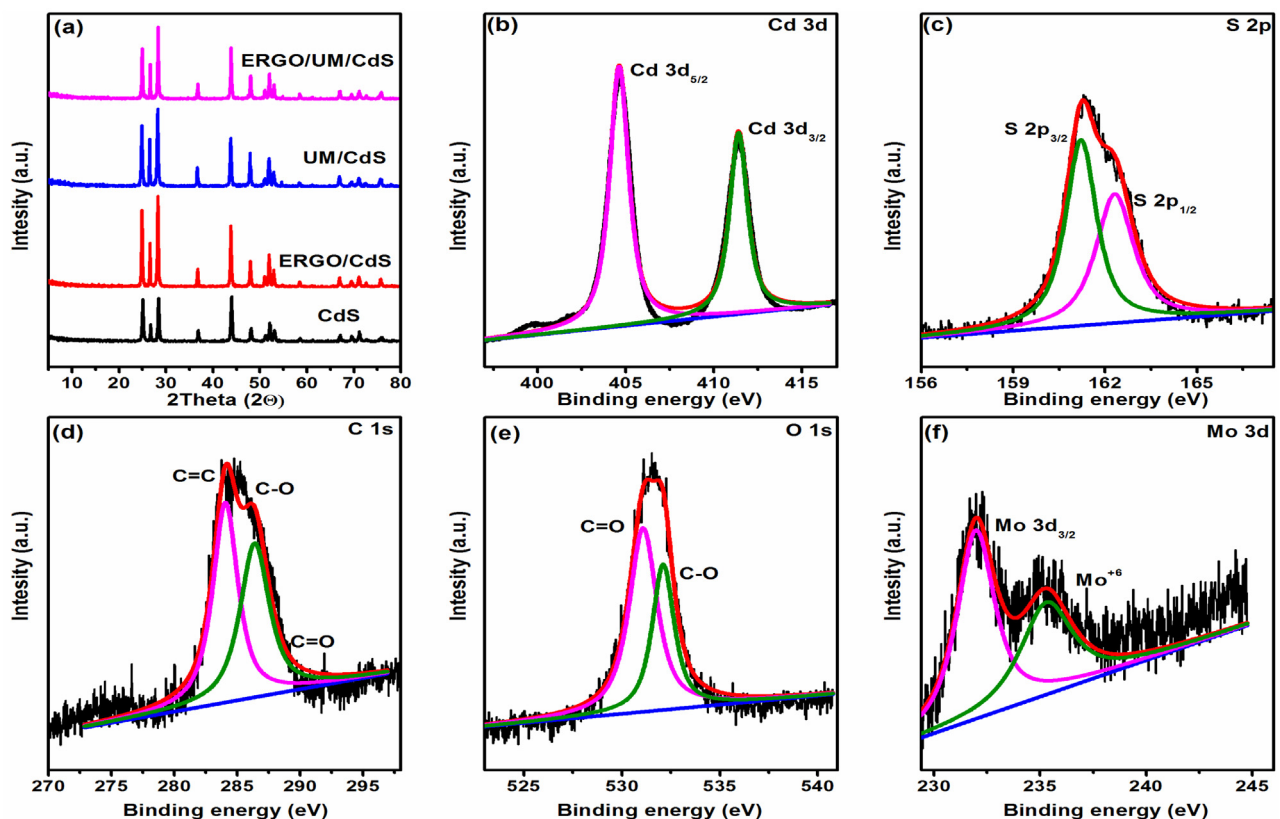


Fig. 1. (a) XRD patterns of Cds and related composites. (b)–(f) XPS spectra of ERGO/UM/CdS composites showing expanded Cd, S, C, O, and Mo regions, respectively.

ence of Cd, Mo, S, C, and O (Fig. S2). The oxidation states of these elements were confirmed by high-resolution Cd 3d, Mo 3d, and S 2p XPS spectra. Fig. 1(b) shows the Cd 3d XPS spectrum, with binding energies of 404.9 and 411.5 eV corresponding to Cd3d_{5/2} and Cd3d_{3/2} transitions, respectively. This result confirms that Cd has an oxidation state of +2 in Cds [48]. In addition, S 2p peaks were detected at 161.2 and 162.5 eV (Fig. 1(c)), while Mo3d peaks at 228.3 (Mo 3d_{5/2}) and 232.0 eV (Mo 3d_{3/2}) confirmed that Mo⁴⁺ was the dominant oxidation state (Fig. 1(f)). The binding energies of Mo and S were in good agreement with the reported values [49], confirming the presence of MoS₂. Finally thus, XPS analysis confirmed the presence of MoS₂ and Cds in the composites. The small peak with a binding energy of ~236 eV was ascribed to the presence of a small amount of Mo⁶⁺ [50]. In Figs. 1(d) and 1(e), the C 1s peak could be

deconvoluted into three peaks. The peak at 284.5 eV confirmed the presence of sp²-hybridized carbon, and the peak at 285.4 eV indicated the presence of C—O, C—S, and C—N bonds [51]. The peak at 288.8 eV was attributed to C=O bonds, demonstrating the presence of residual carbonyl and carboxyl groups [51].

3.3. Morphological analysis

The composite structure and morphology were investigated by transmission electron microscopy (TEM) (Fig. 2). Fig. 2(a)–(e) display exfoliated graphene with integrated ultrathin MoS₂ dispersed on the Cds nanorods. Cds exhibited 1D rod-shaped morphology, being decorated with ultrathin 2D MoS₂ and ERGO nanosheets, as indicated by the red circles and yellow rectangles in Fig. 2(b).

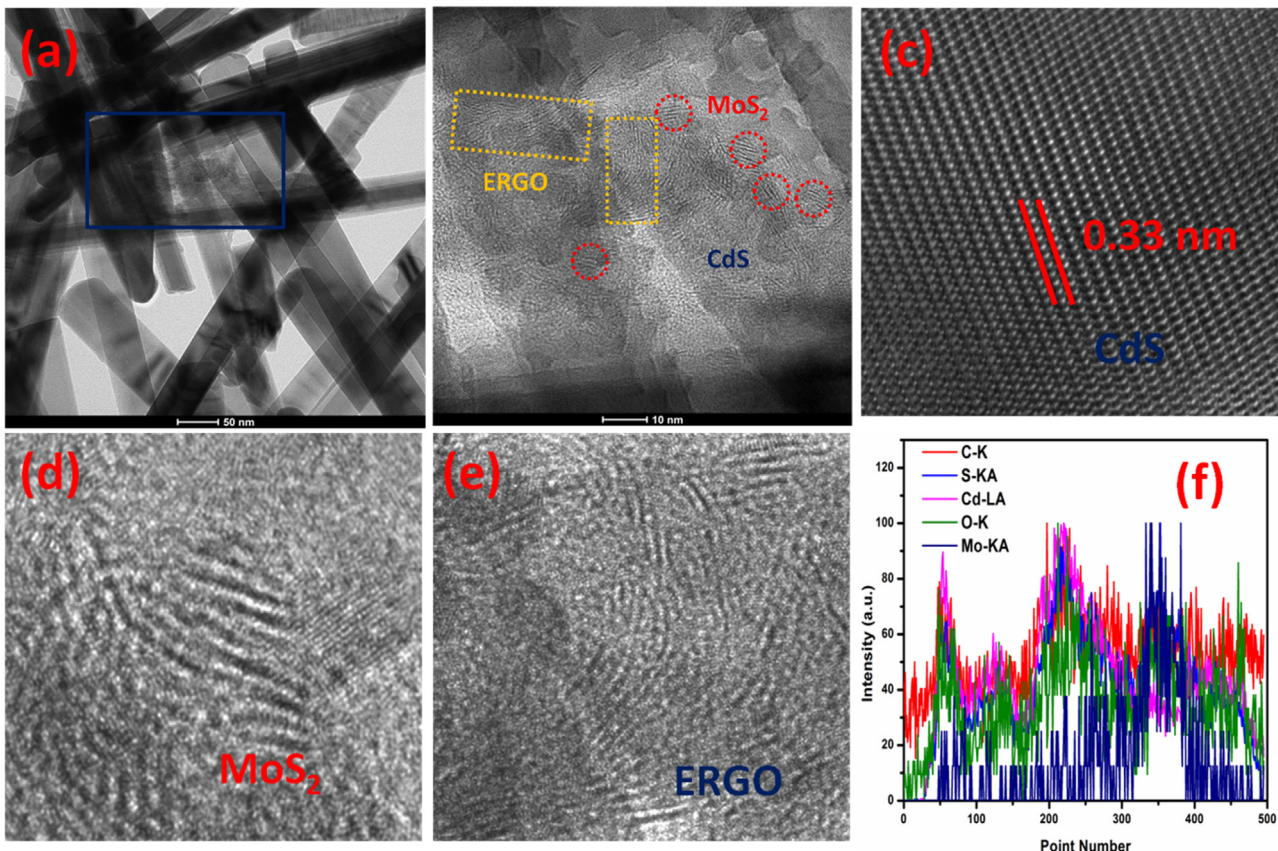


Fig. 2. (a)–(b) TEM and HRTEM images of ERGO/UM/CdS, respectively. (c)–(e) High-magnification HRTEM images of CdS, MoS₂, and ERGO, respectively. (f) Line-scan elemental analysis of ERGO/UM/CdS (Cd, S, C, O, and Mo elements).

High-resolution images of CdS, MoS₂, and ERGO are displayed in Fig. 2(c)–2(e), respectively [51]. The elemental compositions determined by Energy-dispersive X-ray spectroscopy (EDS) mapping are displayed in Fig. S2, confirming the presence of five elements: Cd, Mo, C, O, and S. Fig. 2(f) displays the results of elemental analysis obtained by line scanning. The EDS results confirmed that Mo, C, and O were well-dispersed, being present in much lower amounts than Cd and S due to the much lower weight percentage of MoS₂ and ERGO used for the synthesis of ERGO/UM/CdS. The optical properties of CdS and related composites were investigated by UV–vis diffuse reflectance spectroscopy (Fig. S4). The color of the synthesized nanocomposite samples becomes darker with the increasing ratio of MoS₂ and ERGO to CdS nanorods, changing from light yellow to dark green. The visible light absorption capacity of these composites increases than that of bare CdS due to the effect of deposited co-catalyst (UM and ERGO/UM) better interaction. Further observations indicate that all samples show absorption edges identical to that of pure CdS, implying that ERGO and MoS₂ are not incorporated into the CdS lattice. Moreover, the calculated band gap values of nanocomposites were almost identical to that of pure CdS [51,52]. Therefore, the as-synthesized nanocomposites exhibited a higher solar radiation utilization capacity, leading to better photocatalytic efficiency compared to pure CdS.

3.4. Photoluminescence spectral analysis

Photoluminescence (PL) measurement provide information on the electronic transitions of photocatalysts, using emission spectra recorded upon irradiation with light of a particular wavelength. In this study, the PL spectra of photocatalysts were recorded at an excitation wavelength of 380 nm. Fig. 3(a) shows the PL spectra

of CdS, ERGO/CdS, UM/CdS, and ERGO/UM/CdS. CdS shows distinct bands, probably associated with near-band-edge emission, while the emissions of MoS₂/CdS and ERGO/CdS are attributed to surface defects. According to a previous study [53], the photogenerated carriers are easily transferred to the surface, where electrons are not available for H₂ evolution processes. After loading MoS₂ onto CdS, the intensity of PL emission bands decreased, suggesting fast photoinduced electron transfer. Moreover, the weakened intensity of the emission bands indicates that most surface states are passivated, thereby making electrons available for photocatalytic H₂ evolution [50]. The emission band intensities of ERGO/UM/CdS are significantly smaller than those of UM/CdS and ERGO/CdS, implying that the exfoliated graphene and ultrathin MoS₂ layers facilitate charge carrier transfer processes (making them faster) because of their increased number of surface edge sites, separated layers, and improved conductivity [52].

3.5. Photoelectrochemical (PEC) analysis

To further support the enhanced separation efficiency and charge carrier transportation, indium tin oxide (ITO) electrodes coated with CdS, ERGO/CdS, UM/CdS, and ERGO/UM/CdS nanocomposites were photoelectrochemically examined under simulated sunlight irradiation using a potentiostat. Fig. 3(b) shows the photocurrent responses of bare CdS nanostructures and related nanocomposites with 30 s light on/off cycles. As expected, the ERGO/UM/CdS nanocomposites showed the highest photocurrent intensity compared with bare CdS nanostructures and individual ERGO/CdS and UM/CdS nanocomposites, suggesting a higher separation efficiency of the photoexcited electron-hole pairs. Consequently, more electrons could be captured by protons to form H₂.

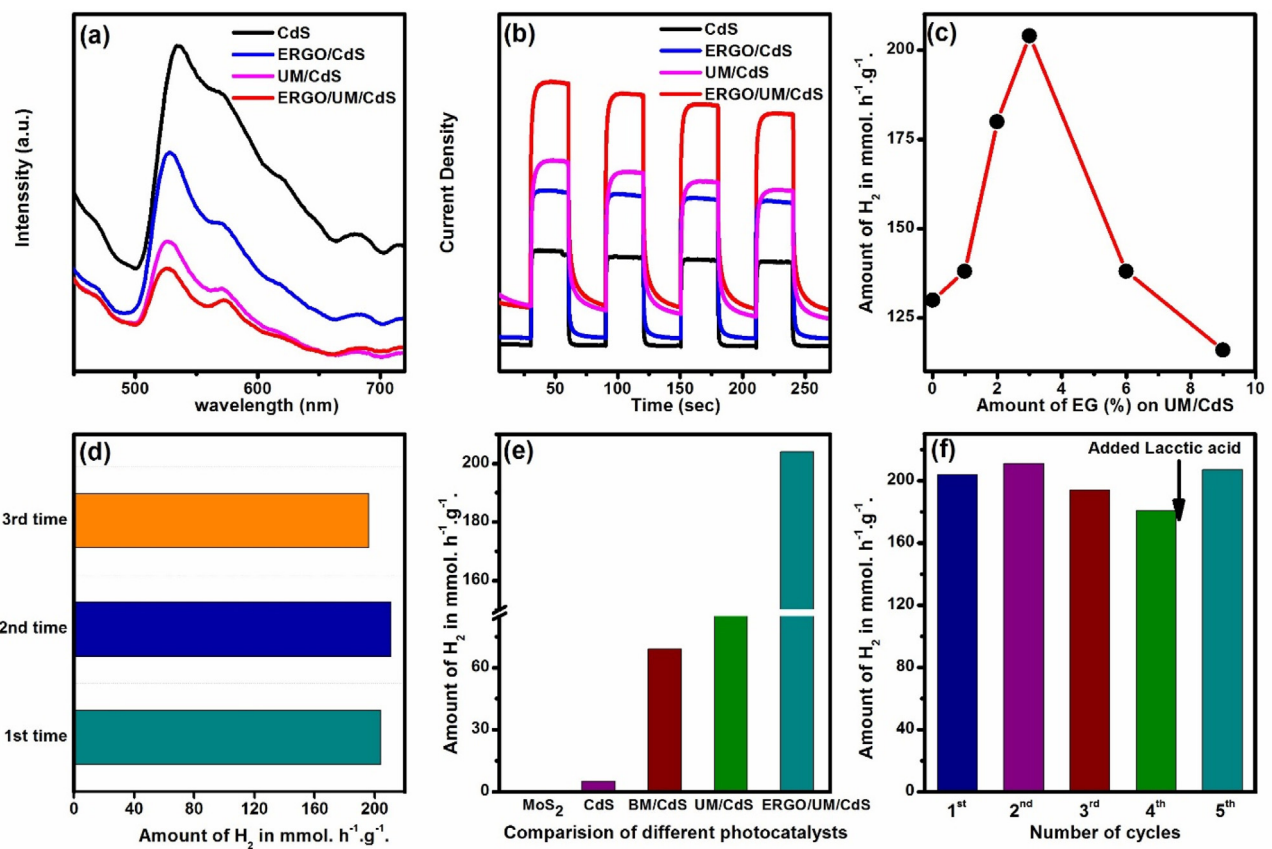


Fig. 3. (a) Photoluminescence spectra of CdS and related composites. (b) Photoelectrochemical characterization of CdS and related composites. (c) Effects of ERGO on UM/CdS. (d) The reproducibility test for ERGO/UM/CdS. (e) The photocatalytic performance comparison of as-synthesized photocatalysts. (f) Recyclability test of 6 wt.% ERGO/UM/CdS, with 1 mg of catalyst dispersed in 15 mL of 20 vol.% aqueous lactic acid solution under simulated solar light irradiation.

Moreover, the photocurrent responses were highly reproducible for several on/off cycles and remained stable, indicating that the exfoliated graphene and ultra-thin MoS₂ on CdS can effectively prevent photocorrosion. These observations were well supported by PL results. Based on the above experimental evidence, one can envision that the ERGO and ultra-thin MoS₂ nanostructures can effectively enhance the photocatalytic activity of CdS nanostructures. The slight decrease photocurrent responses of ERGO/UM/CdS photocatalyst at early time could be ascribed to establishing equilibrium in between electrolyte solution and synthesized material ITO coated electrode layer upon an instant exposure to solar irradiation source. To confirm the stability of photocurrent results, we have analyzed photocurrent measurements for long time range and the data is displayed in Fig. S8. Iqbal et al. [54] also observed the very similar decreases in photocurrent responses at initial time for the case of GaON material.

The presence of ultrathin MoS₂ layers and ERGO nanosheets on CdS nanorods is an important for improved photocatalytic H₂ production. The obtained structural information confirmed the effective separation of MoS₂ and ERGO layers, which confirmed by diffraction patterns and it is dissimilar from those of bulk MoS₂ and pristine graphite. The effective layer separation improved the active sites with higher surface area. The observed morphological properties clearly show that the better deposition of ultrathin MoS₂ and ERGO on CdS nanorods leads to a better interaction one together among three components, benefiting effective charge transportation. The optical properties of the ERGO/UM/CdS composite provide evidence for a more effective solar light utilization compared to BM/CdS and CdS, based on its higher absorption coefficient in the visible region compared to that of other materials. Charge carrier

transfer studies based on PL analyses also confirm the fast migration of carriers in ERGO/UM/CdS without any recombination. The results of photoelectrochemical studies also support the fact that the separation and transportation of charge carriers occur at a higher current density for ERGO/UM/CdS than for ERGO/CdS, UM/CdS, and bare CdS. Hence, these properties of ERGO and UM greatly influence the H₂ production rate of CdS NR under solar light irradiation

3.6. Photocatalytic activity

3.6.1. Effect of MoS₂ dosage on CdS nanorods

The activities of synthesized materials were evaluated for photocatalytic H₂ evolution from water under simulated solar light irradiation, with lactic acid added as a hole scavenger to control the recombination of photogenerated electron-hole pairs. In the present study, we first optimized the content of ultrathin MoS₂ on CdS nanorods, finding that a 6 wt.% loading of UM/CdS leads to a high hydrogen production rate of 135 mmol h⁻¹ g⁻¹ (Fig. S5(a)).

3.6.2. Effect of ERGO dosage on UM/CdS nanorods

The amount of exfoliated graphene on UM/CdS was varied from 0 to 9.0 wt.%, as displayed in Fig. 3(c). The presence of ERGO led to a greater rate of H₂ production, which increased with increasing ERGO loading up to an optimum level of 3.0 wt.%, decreasing at higher loadings. Under optimized conditions, the rate of H₂ production was 204 mmol h⁻¹ g⁻¹, being significantly higher than the rate for UM/CdS. This fact implies that the active edge sites of the ultrathin MoS₂ nanosheets and the superior electrical conductivity of ERGO lead to effective separation of the photogenerated charge carriers and improve the surface shuttling properties for efficient

H_2 production. Lower ERGO loadings resulted in lower rates of H_2 production due to the reduced number of catalytically active sites and poor electrical conductivity. A further increase in the loading of ERGO above the optimum level (i.e., >3.0% ERGO) results in a decrease of the H_2 evolution rate. This reduction of activity can be explained as follows. Coverage of the UM/CdS surface by excess ERGO prevents the exposure to incident light and the generation of electrons from CdS, with excess ERGO possibly acting as a recombination center for the photogenerated electron-hole pairs. The present results were compared with the previously reported ones; where MoS_2 , RGO, and MoS_2/RGO were used as co-catalysts on CdS nanostructures for photocatalytic H_2 evolution (Table S1).

3.6.3. Stability and comparison measurement

To confirm the reproducibility of H_2 production using the optimized catalyst (3 wt.% ERGO/UM/CdS), the experiment was repeated three times, and almost identical results were obtained (Fig. 3(d)). The results for optimized ERGO/UM/CdS were compared with those for pure MoS_2 , CdS, BM/CdS, and UM/CdS, as shown in Fig. 3(e). The rate of H_2 production for 3 wt.% ERGO/UM/CdS was $204\text{ mmol h}^{-1}\text{ g}^{-1}$, which is 40 and 3.0 times greater than that observed for pure CdS ($5\text{ mmol h}^{-1}\text{ g}^{-1}$) and BM/CdS ($69\text{ mmol h}^{-1}\text{ g}^{-1}$), respectively. Recycling experiments were carried out to evaluate the stability of the ERGO/UM/CdS photocatalyst, with results displayed in Fig. 3(f). In these experiments, the rate of H_2 production for the optimized catalyst (3 wt.% ERGO/UM/CdS) was tested for five cycles with 5 h irradiation by simulated solar light. Almost identical amounts of H_2 were produced in all five experiments; although a minor increase was detected in the second cycle due to the better reaction solution adsorption on the catalyst after the first cycle. The third and fourth cycles exhibited a minor decrease of the H_2 production rate, which was attributed to the decreased lactic acid concentration upon its conversion to pyruvic acid during the reaction. It was clearly known that, present reaction mixture solution in acidic medium with pH of 2.06 due to consist of lactic acid as a hole scavenger. We have tested pH of the reaction solution after photo experiment and it also acidic medium with pH of 2.13. Here, we observed the very slight change in pH of the reaction solution and it seems to slightly decrease acidic nature. These slight change in pH of reactions solution is due to the mild oxidation of lactic acid into pyruvic acid. According to earlier reports [55], they also confirmed that the pH of the reaction solutions is different slightly before and after photoreaction was due to the conversion of lactic acid to pyruvic acid.

After the fourth cycle, additional 3 mL of lactic acid solution were added, and the experimental results of the fifth cycle were similar to those of the first cycle. Thus, the catalyst was confirmed to be stable over five cycles. In addition, we calculated the apparent quantum efficiency (QEs) for the optimized ERGO/UM/CdS nanocomposite under visible light irradiation using a 150 W Xe lamp with a 425 nm band pass filter. The quantum yield was estimated to around 47.4%; which is one of the highest QE (%) values than those in earlier reported MoS_2 , RGO and MoS_2/RGO modified CdS semiconductor nanostructures. Comprehensive experimental procedures of QE measurement/calculation were described in SI.

Additionally, we compared the hydrogen production rates with different hole scavengers for optimized ERGO/UM/CdS catalyst and displayed in Fig. S5(b). The scavengers are ethanol (neutral) and triethanolamine (alkaline) other than lactic acid (acidic), we observed the high rate of hydrogen production with lactic acid only. The rate of H_2 productions are 0.5 , 6.57 and $204\text{ mmol h}^{-1}\text{ g}^{-1}$ with respect to ethanol, triethanolamine and lactic acid. Further conducted the photoexperiments with different amounts (1–20 mg) of optimized ERGO/UM/CdS catalyst in reaction solution (in 15 mL) and perceived the rate of H_2 productions are highly difference with respect to amount catalyst in reaction solution. The rate of H_2 pro-

duction for 1, 3, 5, 6, and 20 mg (photocatalyst dose) are 204 , 259 , 307 , and $282\text{ }\mu\text{mol h}^{-1}$ respectively. The H_2 production rate was saturated above than 5 mg in 15 mL reaction solution due to high amount of catalyst leading to shielding effect on suspended catalyst particles. These results were displayed in Fig. S5(c). In addition, we studied the effect of scavenger concentration on the rate of H_2 production for optimized ERGO/UM/CdS catalyst as shown in Fig. S5(d). Initially, the rate of H_2 production was proportional to concentration of lactic acid (up to 5 mL in 15 mL reaction solution, the maximum H_2 production rate of $234\text{ mmol h}^{-1}\text{ g}^{-1}$) and then, an indirect proportional with respect to increasing of scavenger concentration was observed. The decreasing rate of H_2 production is due to the formation of high intermediates at high concentration of lactic acid. In addition, we measured the action spectra of photocatalytic H_2 production by performing photocatalytic experiments for ERGO/UM/CdS catalyst at several different wavelengths between 400 nm and 570 nm. The results are displayed in Fig. S7 in SI. The results of actions spectra reveal that the rate of H_2 productions is vastly differencing with respect to different wavelengths of light source. The high rate of H_2 was observed at cut-off wavelengths filter around 430 nm and after 430 nm, the rate of H_2 production decreases with increasing wavelength towards reaching 570 nm. Hence, it can be speculated that the photocatalytic reactions are determined by the incident light and the light absorption of the photocatalysts directs the rate. In general, the charge carrier's generation during photocatalytic H_2 generation can be occurred, when photocatalyst irradiated with the light having an energy equal to or greater than the band gap of material. These excited charge carriers effectively migrates to undergo proton reduction to H_2 gas generation due to the conduction band potentials of ERGO/UM/CdS is very near and negative than H^+ reduction potentials at $\text{pH}=7$.

3.7. Proposed reaction mechanism

The mechanism of photocatalytic hydrogen production was primarily depends on charge carrier generation and its migration pathways. These charge carrier migrations pathways depend on the conduction band potentials of photocatalytic materials. To derive the exact energy levels of conduction band potentials of as synthesized materials, we have analyzed Mott-Schottky (MS) measurements and determined the possibilities for H^+ reduction to H_2 . The estimated the conduction band potentials of materials from MS measurements at frequency at three different frequencies (0.5 kHz, 1.0 kHz and 2.0 kHz in Fig. S6) were estimated to be -1.12 , -0.87 and -0.68 V (vs. $E_{Ag/AgCl}$ at $\text{pH}=7$) for CdS, UM/CdS and ERGO/UM/CdS, respectively. These results clearly show that the conduction band potential of UM/CdS and ERGO/UM/CdS moved towards H^+ reduction potential -0.607 V vs. ($E_{Ag/AgCl}$ at $\text{pH}=7$) [56]. The ERGO/UM/CdS conduction band potentials are more near than UM/CdS to H^+ reduction potential, which could be ascribed to effects of ERGO and leads to higher photocatalytic efficiency.

A plausible mechanism of efficient H_2 production under solar light irradiation with lactic acid as a hole scavenger and ERGO/UM/CdS as a photocatalyst is depicted in Fig. 4. Excitation of the semiconducting CdS in ERGO/UM/CdS by solar light generates electron-hole pairs in the conduction (CB) and valence bands (VB), respectively [57–59]. The excited electrons may induce proton reduction via three pathways. In the first pathway, the excited electron is transferred to MoS_2 nanosheets and effectively separates the photogenerated holes followed by reduction. The second pathway features the transfer of the excited electron to ERGO nanosheets and effectively separates the photogenerated charge carriers and improves the surface shuttling properties followed by reduction. Finally, the excited electron can be transferred to MoS_2 nanosheets via ERGO nanosheets and effectively separates the photogenerated charge carriers and improves the surface shut-

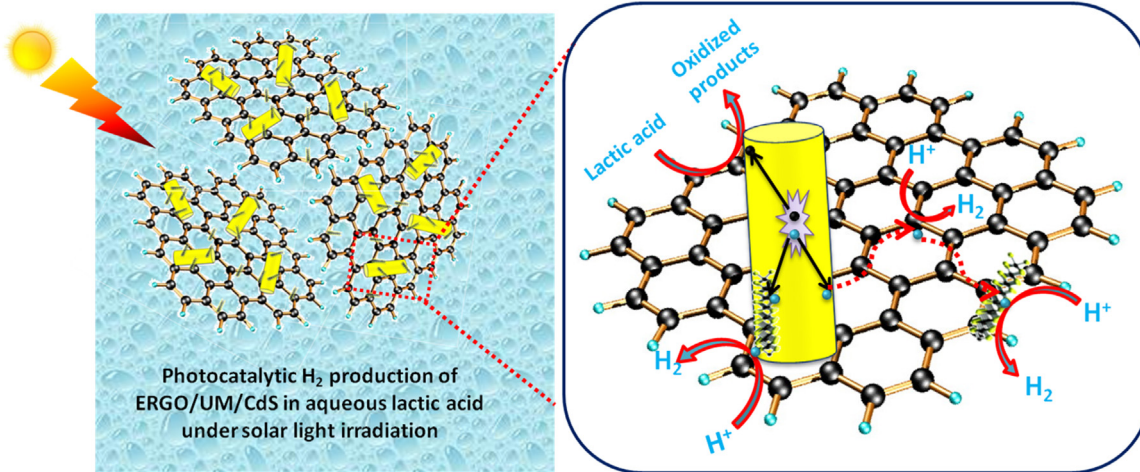


Fig. 4. Schematic representation of the proposed reaction mechanism of ERGO/UM/CdS composite.

tling properties followed by reduction of protons to molecular H_2 . The sacrificial agent (i.e., lactic acid) was oxidized by the photogenerated holes in the VB of CdS. However, the ERGO/UM/CdS composite exhibited superior activity compared to that of bulk MoS₂ nanosheet-decorated CdS nanorods and simple graphene nanosheet-decorated CdS nanorods, due to the ultrathin nature of MoS₂ and exfoliated graphene that strongly hinders the recombination of photogenerated charge carriers and enhances the surface shuttling properties. In addition, the greater number of active edge sites also contributed to the improved adsorption and reduction of protons to produce H_2 .

4. Conclusions

In this study, we have demonstrated that the earth-abundant, noble metal-free ultrathin MoS₂ layers on exfoliated reduced graphene oxides nanosheets hybrid can be used as an efficient co-catalyst for CdS nanorods, achieving extraordinary photocatalytic H_2 production under solar light irradiation. The synergism between ultrathin MoS₂ nanosheets and exfoliated reduced graphene oxide leads to effective separation of the photogenerated charge carriers and improves the surface shuttling properties due to the presence of abundant active edge sites and high electrical conductivity. The ERGO/UM/CdS composites exhibit an extremely high photocatalytic activity, showing the highest H_2 production rates ever reported for RGO and MoS₂ based composites. Hence, this system provides significant motivation for further research of the conversion of solar energy to chemical fuels.

Acknowledgements

This work was supported by National Research Foundation of Korea (NRF) grants funded by the Korean government (MSIP) (2014R1A4A1001690 and 2016R1E1A1A01941978).

Appendix A. Supplementary data

Supplementary data associated with this article can be found, in the online version, at <http://dx.doi.org/10.1016/j.apcatb.2017.04.065>.

References

- [1] J. Chow, R.J. Kopp, P.R. Portney, *Science* 302 (2003) 1528–1531.
- [2] A. Paracchino, V. Laporte, K. Sivula, M. Grätzel, E. Thimsen, *Nat. Mater.* 10 (2011) 456–461.
- [3] A. Fujishima, K. Honda, *Nature* 238 (1972) 37–38.
- [4] X.B. Chen, S.H. Shen, L.J. Guo, S.S. Mao, *Chem. Rev.* 110 (2010) 6503–6570.
- [5] J.R. McKone, N.S. Lewis, H.B. Gray, *Chem. Mater.* 26 (2014) 407–414.
- [6] D.P. Kumar, M.V. Shankar, M.M. Kumari, G. Sadanandam, B. Srinivas, V.D. Kumari, *Chem. Commun.* 49 (2013) 9443–9445.
- [7] D.P. Kumar, N.L. Reddy, M.M. Kumari, B. Srinivas, V.D. Kumari, B. Sreedhar, V. Roddatis, O. Bondarchuk, M. Karthik, B. Nepollian, M.V. Shankar, *Sol. Energy Mater. Sol. Cells* 136 (2015) 157–166.
- [8] A. Kudo, H. Kato, S. Nakagawa, *J. Phys. Chem. B* 104 (2000) 571–575.
- [9] Y. Okamoto, S. Ida, J. Hyodo, H. Hagiwara, T. Ishihara, *J. Am. Chem. Soc.* 133 (2011) 18034–18037.
- [10] H. Kato, A. Kudo, *J. Phys. Chem. B* 105 (2001) 4285–4292.
- [11] K. Wu, Y. Du, H. Tang, Z. Chen, T. Lian, *J. Am. Chem. Soc.* 137 (2015) 10224–10230.
- [12] J. Chen, X. Wu, L. Yin, B. Li, X. Hong, Z. Fan, B. Chen, C. Xue, H. Zhang, *Angew. Chem. Int. Ed.* 127 (2015) 1226–1230.
- [13] R. Marschall, *Adv. Funct. Mater.* 24 (2014) 2421–2440.
- [14] S.E. Habas, P. Yang, T. Mokari, *J. Am. Chem. Soc.* 130 (2008) 3294–3295.
- [15] H. Yan, J. Yang, G. Ma, G. Wu, X. Zong, Z. Lei, J. Shi, C. Li, *J. Catal.* 166 (2009) 165–168.
- [16] J. Yang, D. Wang, H. Han, C. Li, *Acc. Chem. Res.* 46 (2013) 1900–1909.
- [17] C. Han, M.Q. Yang, N. Zhang, Y.J. Xu, *J. Mater. Chem. A* 2 (2014) 19156–19166.
- [18] I.B. Rufus, V. Ramakrishnan, B. Viswanathan, J.C. Kuricose, *Langmuir* 6 (1990) 565–567.
- [19] J. Zhang, J. Yu, M. Jaroniec, J.R. Gong, *Nano Lett.* 12 (2012) 4584–4589.
- [20] Q. Li, B. Guo, J. Yu, J. Ran, B. Zhang, H. Yan, J.R. Gong, *J. Am. Chem. Soc.* 133 (2011) 10878–10884.
- [21] Q.J. Xiang, J.G. Yu, M. Jaroniec, *Chem. Soc. Rev.* 41 (2012) 782–796.
- [22] Q.J. Xiang, J.G. Yu, *J. Phys. Chem. Lett.* 4 (2013) 753–759.
- [23] J.X. Low, S.W. Cao, J.G. Yu, S. Waghé, *Chem. Commun.* 50 (2014) 10768–10777.
- [24] T.T. Jia, A. Kolpin, C.S. Ma, R.C.T. Chan, W.M. Kwok, S.C.E. Tsang, *Chem. Commun.* 50 (2014) 1185–1188.
- [25] Y.G. Li, H.L. Wang, L.M. Xie, Y.Y. Liang, G.S. Hong, H.J. Dai, *J. Am. Chem. Soc.* 133 (2011) 7296–7299.
- [26] T.F. Jaramillo, K.P. Jorgensen, J. Bonde, J.H. Nielsen, S. Horch, I. Chorkendorff, *Science* 317 (2007) 100–102.
- [27] H.I. Karunadasa, E. Montalvo, Y.J. Sun, M. Majda, J.R. Long, C.J. Chang, *Science* 335 (2012) 698–702.
- [28] B. Hinnemann, P.G. Moses, J. Bonde, K.P. Jørgensen, J.H. Nielsen, S. Horch, I. Chorkendorff, J.K. Norskov, *J. Am. Chem. Soc.* 127 (2005) 5308–5309.
- [29] H. Vrubel, D. Merki, X.L. Hu, *Energy Environ. Sci.* 5 (2012) 6136–6144.
- [30] D. Merki, S. Fierro, H. Vrubel, X. Hu, *Chem. Sci.* 2 (2011) 1262–1267.
- [31] D.P. Kumar, S. Hong, D.A. Reddy, T.K. Kim, *J. Mater. Chem. A* 4 (2016) 18551–18558.
- [32] M.A. Lukowski, A.S. Daniel, F. Meng, A. Forticaux, L.S. Li, S. Jin, *J. Am. Chem. Soc.* 135 (2013) 10274–10277.
- [33] U. Maitra, U. Gupta, M. De, R. Datta, A. Govindaraj, C.N.R. Rao, *Angew. Chem. Int. Ed.* 52 (2013) 13057–13061.
- [34] J. Zhang, H.Y. Qi, J.R. Ran, J.G. Yu, S.Z. Qiao, *Adv. Energy Mater.* 4 (2014) 1301925.
- [35] Q.J. Xiang, J.G. Yu, M. Jaroniec, *Nanoscale* 3 (2011) 3670–3678.
- [36] M.J. Allen, V.C. Tung, R.B. Kaner, *Chem. Rev.* 110 (2010) 132–145.
- [37] C. Han, N. Zhang, Y.J. Xu, *Nano Today* 11 (2016) 351–372.
- [38] M.Q. Yang, N. Zhang, M. Pagliaro, Y.J. Xu, *Chem. Soc. Rev.* 43 (2014) 8240–8254.
- [39] N. Zhang, Y. Zhang, Y.J. Xu, *Nanoscale* 4 (2012) 5792–5813.
- [40] N. Zhang, Y.J. Xu, *CrystEngComm* 18 (2016) 24–37.
- [41] Y. Zhang, Z.R. Tang, X. Fu, Y.J. Xu, *ACS Nano* 4 (2010) 7303–7311.
- [42] N. Zhang, M.Q. Yang, Z.R. Tang, Y.J. Xu, *ACS Nano* 8 (2014) 623–633.

- [43] N. Zhang, M.Q. Yang, S. Liu, Y. Sun, Y.J. Xu, *Chem. Rev.* 115 (2015) 10307–10377.
- [44] T. Soltani, B.K. Lee, *J. Colloid Interface Sci.* 486 (2017) 337–343.
- [45] S. Pei, H.M. Cheng, *Carbon* 50 (2012) 3210–3228.
- [46] D.A. Reddy, H.K. Kim, Y. Kim, S. Lee, J. Choi, M.J. Islam, D.P. Kumar, T.K. Kim, *J. Mater. Chem. A* 4 (2016) 13890–13898.
- [47] D.A. Reddy, J. Choi, S. Lee, Y. Kim, S. Hong, D.P. Kumar, T.K. Kim, *Catal. Sci. Technol.* 6 (2016) 6197–6206.
- [48] D.H. Wang, L. Wang, A.W. Xu, *Nanoscale* 4 (2012) 2046–2053.
- [49] J.G. Yu, Y.F. Yu, B. Cheng, *RSC Adv.* 2 (2012) 11829–11835.
- [50] J. He, L. Chen, F. Wang, Y. Liu, P. Chen, C.T. Au, S.F. Yin, *ChemSusChem* 9 (2016) 624–630.
- [51] K. Zhang, W. Kim, M. Ma, X. Shia, J.H. Park, *J. Mater. Chem. A* 3 (2015) 4803–4810.
- [52] M.Q. Yang, C. Han, Y.J. Xu, *J. Phys. Chem. C* 119 (2015) 27234–27246.
- [53] D.S. Kong, H.T. Wang, J.J. Cha, M. Pasta, K.J. Koski, J. Yao, Y. Cui, *Nano Lett.* 13 (2013) 1341–1347.
- [54] N. Iqbal, I. Khan, Z.H. Yamani, A. Qurashi, *Sci. Rep.* 6 (2016) 32319.
- [55] W. Zhang, Y. Wang, Z. Wang, Z. Zhong, R. Xu, *Chem. Commun.* 46 (2010) 7631–7633.
- [56] D. Lang, T. Shen, Q. Xiang, *ChemCatChem* 7 (2015) 943–951.
- [57] L. Shang, B. Tong, H. Yu, G.I.N. Waterhouse, C. Zhou, Y. Zhao, M. Tahir, L.Z. Wu, C.H. Tung, T. Zhang, *Adv. Energy Mater.* 6 (2016) 1501241–1501248.
- [58] B. Qiu, Q. Zhu, M. Xing, J. Zhang, *Chem. Commun.* 53 (2017) 897–900.
- [59] B. Qiu, Q. Zhu, M. Du, L. Fan, M. Xing, J. Zhang, *Angew. Chem. Int. Ed.* 56 (2017) 2684–2688.